Loading- and substructure-induced irreversibility in texture during Route C Equal Channel Angular Extrusion

S. Mahesh[a], I. J. Beyerlein[b], C. N. Tomé[c]

[a]Departments of Aerospace and Mechanical Engineering, Indian Institute of Technology, Kanpur 208016. India

[b]Theoretical Division, Los Alamos National Laboratory, Los Alamos NM 87545. USA

[c]Materials Science and Technology Division, Los Alamos National Laboratory, Los Alamos NM 87545. USA

The experimental texture after two Equal Channel Angular Extrusion (ECAE) passes by route C differs qualitatively from that calculated using standard polycrystal models assuming forward and reverse simple shear. Agreement between orientation imaging microscopy (OIM) measured textures of ECAE copper and polycrystal model calculations is obtained by accounting for strain hardening, substructure formation, and non-uniform distribution of the bulk deformation.

Keywords: plastic deformation, extrusion, load path reversal, texture, copper

1. Introduction

Much recent research has focused on equal channel angular extrusion (ECAE), a promising technology for producing bulk nano-crystalline materials [1]. During ECAE, a billet is repeatedly passed through a die consisting of two equal channels intersecting at an angle Φ wherein it undergoes large shear deformations. It has been experimentally found [2,3] that the sequence of rigid rotations applied to the billet before reinsertion for the next pass (ECAE route) and the number of passes significantly influence the degree of grain refinement.

ECAE deformation is said to follow route C when rigid rotations of 180° about the billet axis, followed by a rotation to align the billet axis with the entry channel (e.g., 90° about an axis perpendicular to the plane of the die when $\Phi = 90°$) is applied between passes. Equivalently, route C deformation may be regarded as extrusion through two identical $\Phi = 90°$ dies oriented as shown in Fig. 1 with the billet passing from the outlet channel of the first die to the inlet channel of the second without rotations. Throughout we consider dies with $\Phi = 90°$ and impose route C as in Fig. 1.

Deformation in each pass is most often approximated as concentrated simple shearing on the intersection plane of the channels [1]. A better approximation [4–6] consists of distributed simple shearing in a fan-shaped region of the die. For either ideal simple shear or an ideal fan, the deformation by consecutive passes in route C results in repeated forward and reverse shear, so that the deformation of even passes exactly reverses that of the previous odd-pass deformation. Accordingly, a Taylor polycrystal calculation assuming any deformation zone that is symmetrically disposed about the die corner will predict that the texture after pass 2 reverts to the initial texture before pass 1. Exact recovery of the initial texture occurs in the model because in grain orientation space, each Taylor grain exactly retraces its first-pass path during its second-pass deformation.

Li et al [7] have recently reported experimental textures after different number of route C passes obtained by local OIM at different stations along the billet diameter. Their die had a rounded outer corner, promoting deformation over a fan-shaped deformation zone. The measured texture after two route C passes shows shear-type texture features seen after one pass. Similarly large

strain torsion tests on fcc materials have also reported shear-type textures after reversal [8,9], which have been called the "retained shear texture".

In this work we show that in order to explain the experimental retained texture after two passes, it is necessary to simultaneously account for (i) strain hardening behavior in the material, (ii) substructure formation in the grains, and (iii) non-uniform distribution of bulk deformation among grains.

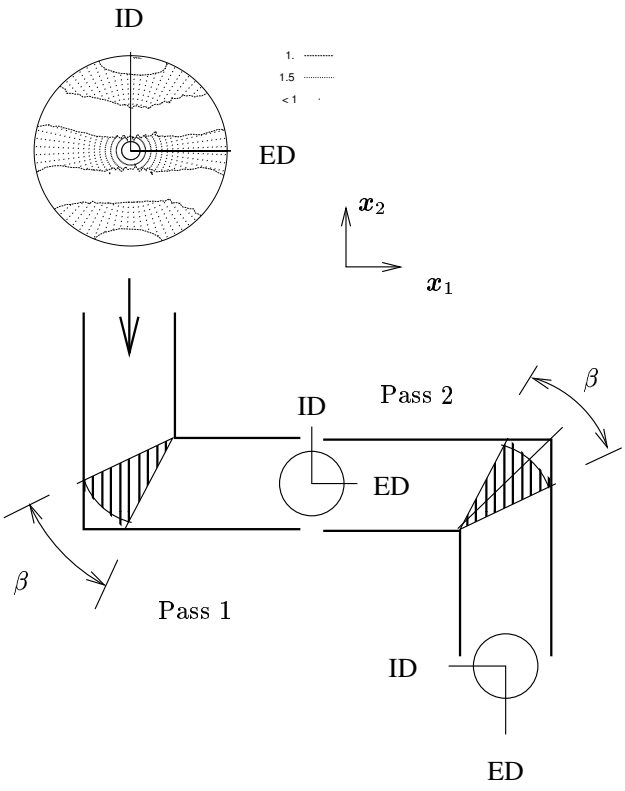

Figure 1. Schematic of two passes of route C ECAE deformation. Shear deformation occurs in the fan-shaped region (hatched) subtending angle β at the inner corner of the die. The (111) pole figure of the measured initial texture of the material is also shown.

2. Texture after two passes of route C

2.1. Experimental Observations

The first row in Fig. 2 shows the experimental (111) pole figures of the texture reported by Li et al [7] using OIM analysis close to the central axis of the billet after the first and second pass of route C ECAE on copper. In Fig. 2, contour lines are spaced at intensities of 1, with 1 being the random texture intensity. Level 1 occurs in all rows and columns. Dots denote regions of intensity less than 1. The insertion direction (ID) and extrusion direction (ED) are $(\mathrm{ED}, \mathrm{ID}) = (\boldsymbol{x}_1, \boldsymbol{x}_2)$ after pass 1, and $(\mathrm{ED}, \mathrm{ID}) = (-\boldsymbol{x}_2, -\boldsymbol{x}_1)$ after pass 2 as shown in Fig. 1. The initial texture of their material is shown in Fig. 1. Three texture components labeled ①, ②, and ③ occur after pass 1 and pass 2. Note that the pole figure has two-fold symmetry: e.g., ① labels two orientation concentrations diametrically opposite each other.

2.2. Modeling approach

All other rows in Fig. 2 contain (111) pole figures showing texture predictions using polycrystal plasticity calculations. Pole figures are plotted at the end of pass 1 and 2 in columns 1 and 2, respectively. All calculations start with the same set of 1581 grains reproducing the initial texture shown in Fig. 1 and deforming according to the visco-plastic constitutive law: If $\dot{\boldsymbol{\epsilon}}$ is the strain rate imposed on a grain whose S slip systems indexed by s have unit normals $\boldsymbol{n}^s$ and Burgers vectors $\boldsymbol{b}^s$ respectively, the grain visco-plastic constitutive response is taken as [10,11]

$$\dot{\boldsymbol{\epsilon}} = \sum_{s=1}^{S} \boldsymbol{m}^s \left| \frac{\boldsymbol{\sigma} : \boldsymbol{m}^s}{\tau^s} \right|^n \mathrm{sign}(\boldsymbol{\sigma} : \boldsymbol{m}^s), \qquad (1)$$

where $\boldsymbol{\sigma}$ is the grain stress, τ^s is the critical resolved shear stress of slip system s, n is the reciprocal rate sensitivity ($n = 20$ in this work), and the Schmid tensor $\boldsymbol{m}^s$ of slip system s is given by

$$\boldsymbol{m}^s = (\boldsymbol{n}^s \otimes \boldsymbol{b}^s + \boldsymbol{b}^s \otimes \boldsymbol{n}^s)/2. \qquad (2)$$

Grains are allowed to harden according to the extended Voce model of Tomé et al [12]; that is, τ^s evolves with accumulated grain strain Γ according to

$$\tau^s = \tau_0 + (\tau_1 + \theta_1 \Gamma)[1 - \exp(-\theta_0 \Gamma / \tau_1)]. \qquad (3)$$

				Intensity		
row	model	banding?	ϕ(rad)	①	②	③
Expt	–	–	–	3	4	2
A	T	no	0	2	0	0
B	SC	no	0	2	2	0
C	T	yes	0	1	3	4
D	T	no	$\pi/50$	4	3	5
E	T	yes	$\pi/50$	3	4	5
F	SC	no	$\pi/50$	6	8	5

Table 1
Model parameters used in calculating the pole figures shown in Fig. 2 (columns 2–4), and intensities of the three texture components after pass 2 (columns 5–7). T in column 2 denotes the Taylor model, and SC the self-consistent model. Fan angle $\beta = \pi/10$ for all cases.

The parameters of this model are fit to the compression stress-strain curve in [12] starting from a random texture to obtain $\tau_0 = 16$ MPa, $\tau_1 = 90$ MPa, $\theta_0 = 180$ MPa, and $\theta_1 = 4$ MPa. The only deformation mode considered for the copper grains is $\langle 110 \rangle (111)$ slip.

The velocity gradient imposed upon the polycrystal corresponds to deformation in a fan-shaped region and is taken according to the model of Segal [4] and Beyerlein and Tomé [5]. Unless stated otherwise the fan-shaped region is assumed symmetrically disposed about the intersection plane of the die as shown in Fig. 1. In the following calculations, the internal fan angle β is fixed at $\beta = \pi/10$. This value gives good agreement with the one- to four-pass textures measured in Cu and Al [13], both processed by the same rounded corner die [14] used to process the copper results in Fig. 2. For the calculations presented here we use the Visco-Plastic Self-Consistent (VPSC) polycrystal plasticity code [18], either in the Taylor full-constraints mode or in the self-consistent mode. The deformation history is read into the code. When required, a version of VPSC incorporating the banding model of Mahesh and Tomé [19] is used for studying the effect of grain sub-structure on texture development.

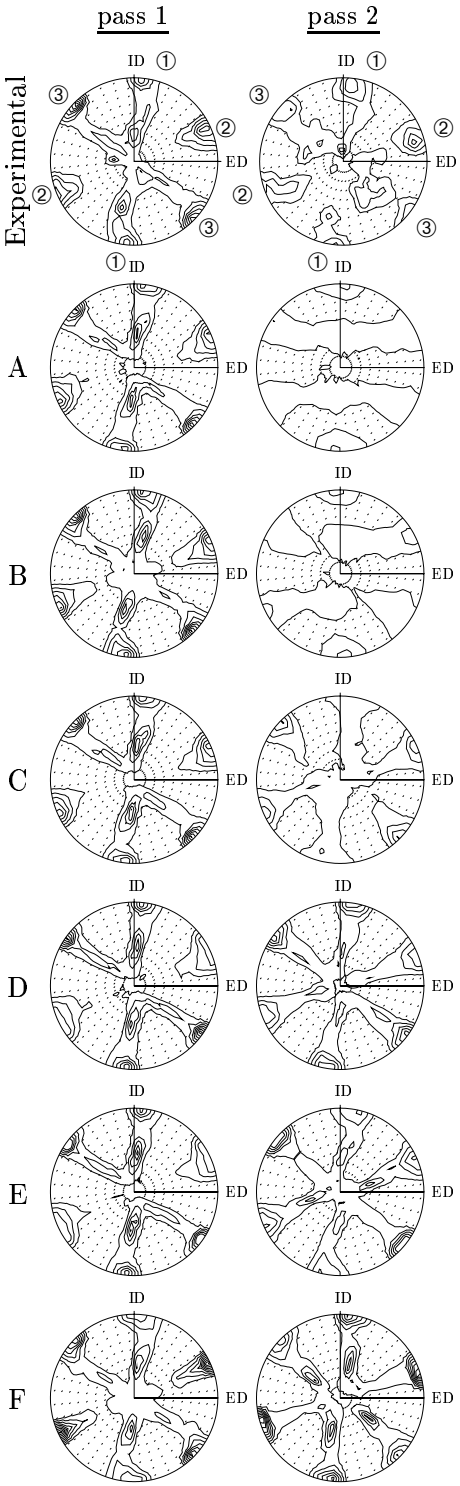

Figure 2. (111) pole figures of copper from experiment (first row), and as calculated under various assumptions (rows A-F) summarized in Table 1. $\beta = \pi/10$ throughout. Contour levels: 1, 2, ...

2.3. Standard Model Predictions

Row A of Fig. 2 shows the (111) texture pole figures obtained from a Taylor polycrystal calculation [15,16] wherein the velocity gradient imposed on each grain equals the velocity gradient imposed upon the polycrystal. After pass 1, the predicted texture agrees qualitatively well with the measured texture although the texture intensities are too high compared with the measurement[1]. However, after pass 2 the Taylor prediction reverts to the initial texture because each Taylor grain exactly retraces its first pass path in the course of its second pass deformation. This happens despite different hardening profiles during the forward and reverse passes, as given by Eq. 3.

It may be argued that if the Taylor assumption of deformation uniformity at the level of individual grains was relaxed then the initial texture may not be recovered. To prove this is not the case, row B shows the texture evolution calculated using the viscoplastic self-consistent polycrystal approach [18]. Unlike the Taylor approach, the self-consistent model does not impose the macroscopic velocity gradient upon each grain. Instead, grain strain rate is determined self-consistently by embedding the grain in a homogeneous effective medium whose properties are the average properties of all the grains. The present calculation accounts for individual grain shape evolution with deformation. Thus grains will not exactly retrace their pass 1 path in orientation space during pass 2. In spite of this improvement it is clear that the self-consistently calculated texture after pass 2 (row B second column) is still almost identical to the initial texture.

2.4. Predictions with Deformation Banding

A possible reason for the failure of the standard models in predicting the pass 2 texture is that although physical grains deform inhomogeneously as they develop dislocation substructures under large strains, the model grains deform homogeneously. Substructure development subdivides the grains into smaller bands, and the band misorientation evolves with strain such that grains evolve a sub-grain texture of their own. Because the substructures developed in the first pass persist during second pass deformation, their formation introduces an irreversibility that prevents grain orientations in pass 2 from retracing their pass 1 paths, as in row A. The recently developed theory of deformation banding [19] models grain substructure formation. Deformation banding is assumed to occur if it causes a reduction in the overall plastic power of the grain and if the plastic power component associated with accommodating disparately deforming parts (i.e. the bands) does not exceed the reduction in the overall plastic power. In the present calculations, first generation bands formed from grains are allowed to band again according to the same criterion.

Row C shows the textures predicted by accounting for deformation banding. As in rows A and B, the pass 1 texture is in good agreement with the measurements. There is also a non-negligible pass 2 texture, although as seen from Table 1, the ordering of texture intensities in the three regions of orientation concentration differs between prediction and measurement (predicted: ① < ② < ③ vs. measured: ③ < ① < ②). Also as seen from Table 1, the predicted texture intensity at ① is much too small.

2.5. Predictions with Skewed Fan

Another possible reason why the standard models fail to predict the 2-pass textures is that the ECAE deformation is different between the first and second pass due to a difference in material behavior. Using finite element simulation of the ECAE process, Li et al [20, Fig. 11] studied the characteristics of plastic deformation zones generated assuming perfectly-plastic and strain-hardening material behavior. While the plastic deformation zones were approximately fan-shaped in all cases, the equivalent strain rate fields were symmetric about the intersection plane of the channels for a perfectly plastic material and asymmetric for the strain-hardening material. In the latter, the plane of symmetry was tilted toward the outlet channel. To capture the influence of strain hardening in the Cu during the

[1] The predicted and measured maximum texture intensities are 5 and 2.8, respectively. The tendency of Taylor calculations to over-predict grain rotations is well known [17].

first pass, we tilt the deformation fan through an angle ϕ toward the outlet channel with respect to the die. During the second pass, the material is expected to harden much less, so no tilt is required.

Row D shows the textures calculated by tilting the deformation region in the pass 1 die through $\phi = \pi/50$ radians about the $\boldsymbol{x}_3$ axis, and leaving the deformation region in the pass 2 die untilted. This calculation assumes a Taylor model for the polycrystal and no banding. The so calculated pass 2 texture has a sizable ① intensity and the intensities are ordered as ② < ① < ③. As seen from Table 1, this is not in agreement with the experimental observation showing highest intensity at ②. Accounting for deformation banding improves the agreement in row E by mending one of the inequalities. Now the calculated intensities order as ① < ② < ③. Notably, the peak values of intensities have reduced and are closer to those in the OIM pass 2 texture.

Still, it is found that contrary to the measurement, ③ has the highest texture intensity. An indication of the source of discrepancy is obtained by repeating the calculation with the self-consistent model without banding, with a first pass tilt of $\phi = \pi/50$. Row F shows the calculated texture, and it is seen from Table 1 that ② does indeed have the highest texture intensity as in the measured texture. This suggests that the discrepancy in strength of some texture components in the row E texture originates from the Taylor assumption.

3. Discussion

Row F shows that the self-consistent model, in combination with the tilt ϕ to model strain hardening in pass 1, captures both the position and intensity orderings of the orientation concentrations. The magnitudes of the intensities however are excessively high in row F. Allowing for deformation banding reduces the intensities, which is demonstrated by comparing rows D and E. Banded grains introduce additional texture components which serve to spread the final material texture. Unfortunately though, the present version of deformation banding cannot be implemented within the self-consistent scheme. Because, if grain deformation is allowed to be inhomogeneous and required to follow the path of least plastic power, it can be shown that the positive definiteness of the grain tangent modulus is destroyed, which in turn destroys convergence of the self-consistent scheme.

It should be noted that it is not directly the incorporation of hardening given by Eq. (3) in the polycrystal model that is important for texture retention in rows D–F. Rather, this important effect is reproduced by (i) incorporating the correct strain path, which is slightly modified by hardening during pass 1, and (ii) the nucleation of bands which is promoted by rapid hardening during pass 1 [19]. The influence of (i) is stronger than that of (ii), as seen by comparing rows D and E.

The pass 1 tilt $\phi = \pi/50$ in rows D, E, and F is very small suggesting the sensitivity of the retained texture to the asymmetry of deformation. This sensitivity is related to the smallness of $\beta = \pi/10$: since most of the deformation during a pass is concentrated in a small region, the slight tilt of the fan suffices to produce enough asymmetry between forward and backward loading to leave a shear texture after pass 2. If β were larger, a larger ϕ would be needed for the same purpose.

Fig. 3 shows the misorientation distribution between bands calculated using the parameters of row E, after passes 1 and 2. While misorientation data across deformation bands in copper after two route C passes is unavailable, McNelley and Swisher [21] have found that 40–70% of all deformation band boundaries have misorientations of 2–5° after pass 1 in pure fcc Al. Comparably, 68% of the misorientations in Fig. 3 are predicted between 2–5° after pass 1. [21] also reports misorientations $\geq 40°$ in Al after four passes along route B_c. Though this information cannot be quantitatively compared with the present calculations because of loading path and material differences, we note from Fig. 3 that comparably large calculated misorientations begin to emerge already after two route C passes. Finally, the calculated misorientation histogram widens with further deformation, in agreement with the experimental trend across deformation bands [21], and

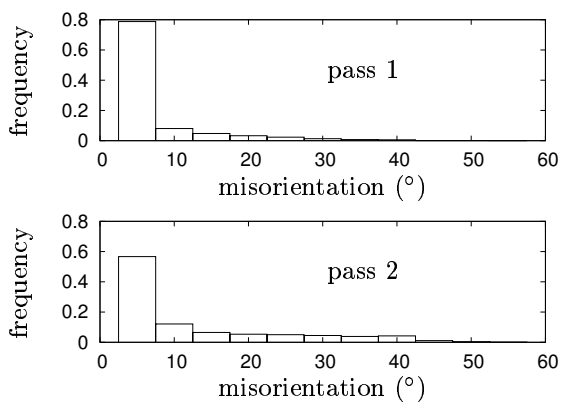

Figure 3. Calculated misorientation distribution between bands after the first and second passes of route C ECAE showing widening of the distribution in the second pass. The ordinate is normalized to 1 in plotting both histograms.

also across smaller dislocation structures [2,7].

4. Conclusions

It has been shown that to explain the shear-type texture after two route C ECAE passes one must account for (i) strain hardening behavior in the material, (ii) substructure formation, and (iii) non-uniform distribution of the applied bulk deformation among grains. The effect of strain hardening behavior is mimicked here by tilting the plastic deformation zone fan with respect to the die. The key idea is to introduce irreversibility in the deformation history due to differences in hardening behavior of the material between the first and second passes. Substructure formation is accounted for approximately by allowing deformation banding. The self-consistent model is shown superior to the Taylor model. By allowing deformation inhomogeneity among grains, the self-consistent model succeeds where the Taylor model fails: in calculating the ordering of intensities of the texture components after pass 2.

REFERENCES

1. Segal VM. Mater. Sci. Engng. A 1995:A197:157.
2. Iwahashi Y, Horita Z, Nemoto M, Langdon TG. Acta mater, 1998:46:3317.
3. Zhu YT, Lowe TC. Mater. Sci. Engng. A, 2000:A291:46.
4. Segal VM. Mater. Sci. Engng. A, 2003:A345:36.
5. Beyerlein IJ, Tomé CN. Mater. Sci. Engng. A, 2004:A380:171.
6. Tóth LS, Massion RA, Germain L, Baik SC, Suwas S. Acta Mater., 2004:52:1885.
7. Li S, Beyerlein IJ, Necker CT, Alexander DJ. On the development of microstructure and texture heterogeneity in the "strain reversal" route of ECAE. Submitted to Acta Mater., 2005.
8. Backofen WA. Trans AIME, 1950:188:1454.
9. Lowe TC, Lipkin JJ. Mech. Phys. Solids, 1991:39:417.
10. Asaro RJ, Needleman A. Acta metall., 1985:33:923.
11. Canova GR, Fressengeas C, Molinari A, Kocks UF. Acta Metall., 1988:38:1961.
12. Tomé CN, Canova GR, Kocks UF, Christodoulou N, Jonas JJ. Acta metall., 1984:32:1637.
13. Li S, Beyerlein IJ, Alexander DJ. Scripta Mater., 2005:52:1099.
14. Li S, Beyerlein IJ, Necker CT, Alexander DJ, Bourke MAM. Acta Mater., 2004:52:4859.
15. Taylor GI. J. Inst. Met., 1938:62:307.
16. Hosford WF. The mechanics of crystals and textured polycrystals. New York: Oxford University Press; 1993.
17. Hirsch J, Lucke K, Hatherly M. Acta metall., 1988:36:2905.
18. Lebensohn RE, Tomé CN. Acta metall. mater, 1993:41:2611.
19. Mahesh S, Tomé CN. Phil. Mag., 2004:84:3517.
20. Li S, Bourke MAM, Beyerlein IJ, Alexander DJ, Clausen B. Mater. Sci. Engng. A, 2004:A382:217.
21. McNelley TR, Swisher DL. In Y. T. Zhu et al., editor, *Ultrafine Grained Materials III*, pages 89–94, Warrendale: TMS, 2004.